Materials Letters: X 6 (2020) 100041

Contents lists available at ScienceDirect

Materials Letters: X

journal homepage: www.elsevier.com/locate/mlblux

Sharp photoluminescence of Pr^{3+} ions in yttrium oxyfluoride nanospheres: Thermographic phosphor characteristics using the fluorescence intensity ratio technique

J. Suresh Kumar *, K. Pavani, M.P.F. Graça, M.J. Soares

I3N & Physics Department, University of Aveiro, 3810-193, Aveiro, Portugal

ARTICLE INFO

Article history:
Received 30 July 2019
Received in revised form 11 December 2019
Accepted 5 February 2020
Available online 6 February 2020

Keywords:
Thermographic phosphors
Photoluminescence
Nanoparticles
Fluorescence intensity ratio technique

ABSTRACT

YOF:Pr nanoparticles prepared by Pechni sol-gel method were investigated for temperature sensing in this work. Structural investigation such as XRD, Raman, SEM and EDS were done. Photoluminescence experiments at ambient temperature for three different concentrations and with variation in temperature were performed for application in fluorescence intensity ratio (FIR) technique. The FIR of the thermally coupled levels (TCL) $^3P_0$ and $^3P_1$ was determined with respect to temperature and found that the relative sensitivity of the material is 9.37 and 0.87% K^{-1} at 90 and 300 K, respectively. Results proved that Pr^{3+} in YOF nanoparticles can be used for non-contact temperature determination.

1. Introduction

Corrosion-resistant materials with different functional properties are highly essential for specific rude environments, for example, fluorine plasma experiments etc. Rare earth oxyfluorides especially yttrium oxyfluoride (YOF) is a highly corrosion-resistant material [1,2]. Determination of temperature at certain highly corrosive environments like fluorine plasma experiments is a challenging task due to deterioration of material at the contacts. A non-contact way of determining the temperature would be more favourable for those types of environments.

Among different rare-earth ions, Pr^{3+} is one of them that has the ability to emit in the visible region with blue excitation. Particularly, the ion is having two thermally coupled levels (TCL) viz. $^3P_0$ and $^3P_1$ that do alter their emission intensities with temperature. This property could be used to monitor the working temperature using the fluorescence intensity ratio (FIR) technique [3]. Nanoparticles on the other hand encounter many losses in the form of phonon dissipation due to their smaller size and large surface area which is vulnerable to the external environment [4]. In spite of the small size of the nanoparticles, in this work, sharp photoluminescence arising from the TCL of Pr^{3+} were reported along with temperature sensing ability of the YOF:Pr nanoparticles.

2. Experimental

YOF nanoparticles doped with different concentrations (1, 2 and 5 mol%) of Pr^{3+} ions were prepared by sol-gel method. Nitrate precursors of yttrium, praseodymium were used along with ammonium fluoride as a fluoride substitute. Ample amount of citric acid was added to de-ionised water containing stoichiometric amounts of metal nitrates and ammonium fluoride. Ethylene glycol was used as a gelating agent. The solution of the ingredients was gelified at 100 °C after continuous stirring for 12 h. The gel was calcined at 250 °C for 4 h and sintered at 600 °C for 2 h.

The crystal structure of the prepared samples was identified by X-ray diffraction (XRD) using Philips PANalytical Xpert Pro analyser with Cu-Kα radiation. Raman spectrum of host YOF was measured by Jobin Yvon HR800 spectrometer with a 532 nm laser excitation source in reflection mode. The morphology and elemental analysis of prepared phosphor powders were investigated by Hitachi SU-70 scanning electron microscopy (SEM) coupled with Bruker Quantax 400 (B-U) EDS. Luminescence excitation and decay analysis were made on a Horiba Jobin Yvon Fluorolog-3 instrument. Temperature-dependent photoluminescence was measured in the Jobin Yvon HR800 spectrometer equipped with

* Corresponding author.
E-mail address: suresh@ua.pt (J. Suresh Kumar).

https://doi.org/10.1016/j.mlblux.2020.100041
2590-1508/

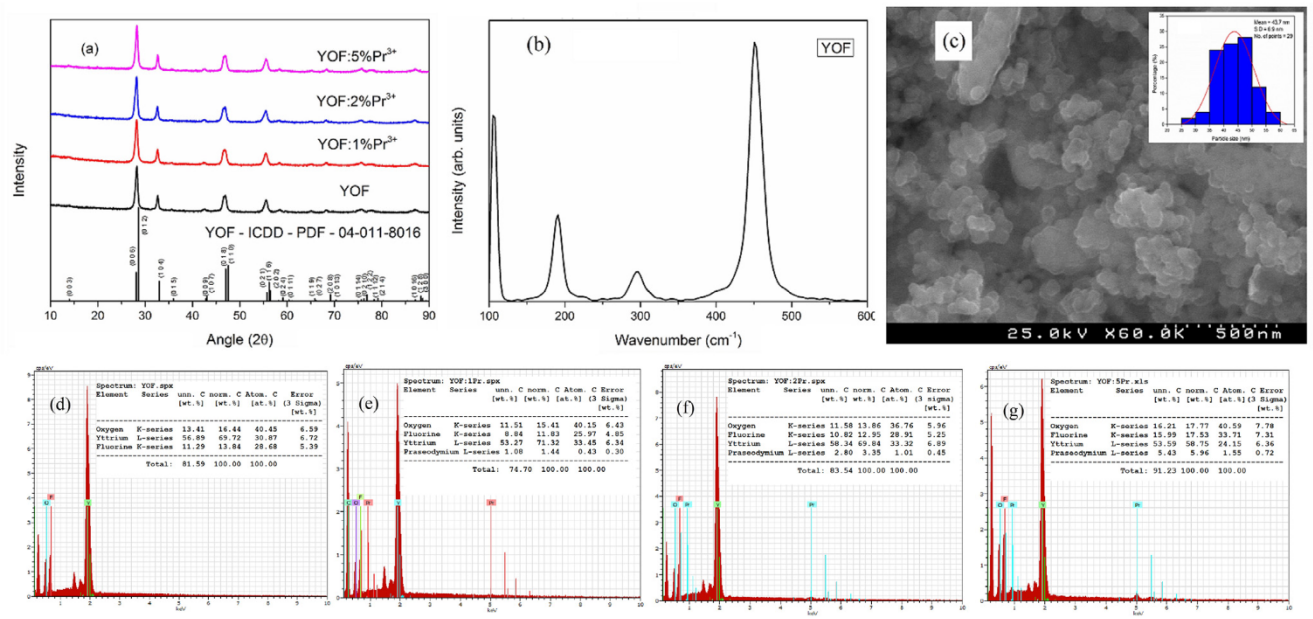

Fig. 1. (a) X-ray diffraction pattern of prepared YOF nanoparticles with and without dopants along with the standard JCPDS data, (b) Raman spectrum of YOF host material, (c) SEM image of YOF nanoparticles with particle size distribution curve as inset and energy dispersion spectra of (d) YOF, (e) YOF: 1% Pr^{3+}, (f) YOF: 2% Pr^{3+} and (g) YOF: 5% Pr^{3+}.

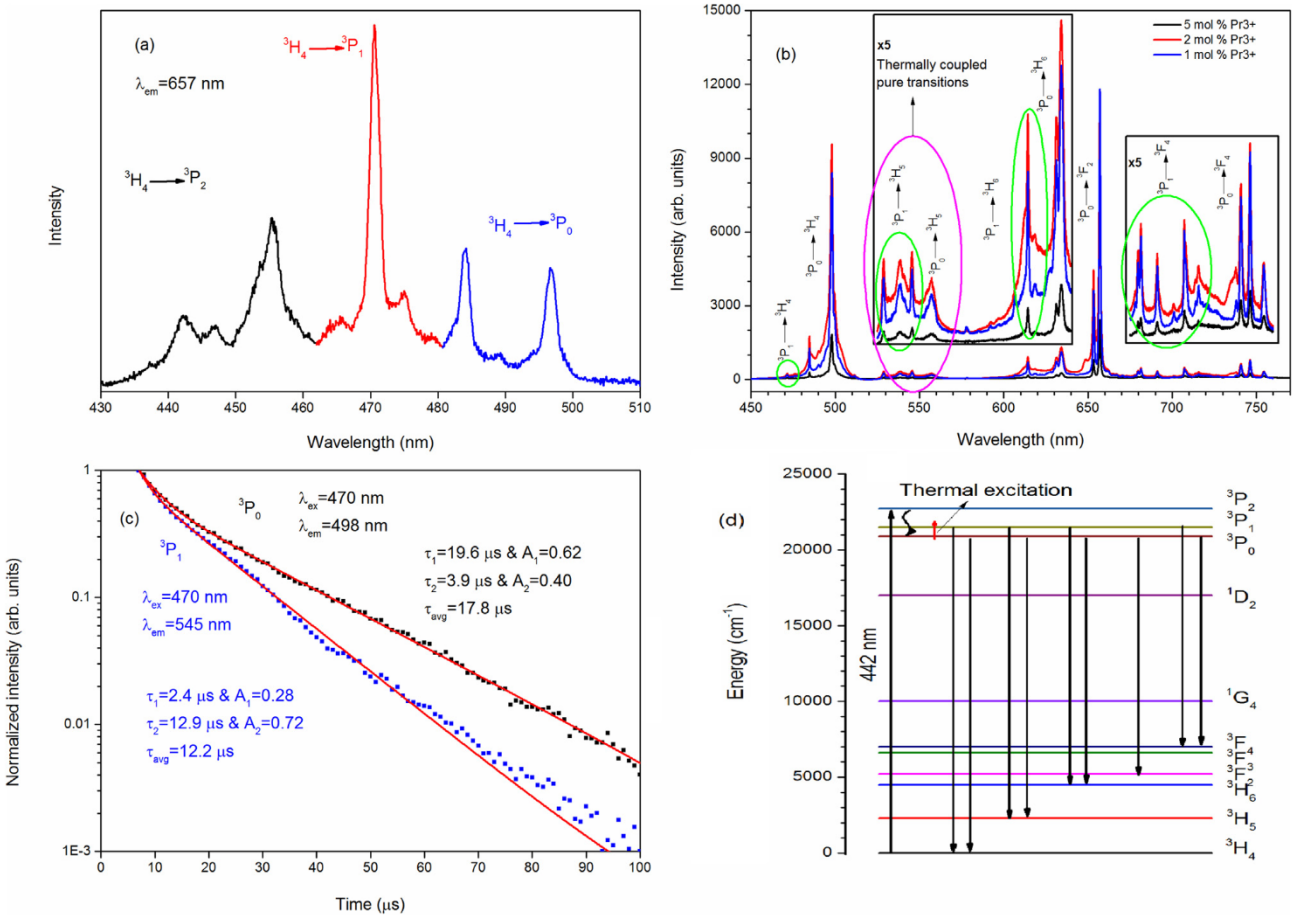

Fig. 2. (a) Excitation spectrum of 2 mol% Pr^{3+} ions, (b) concentration-dependent photoluminescence spectra, (c) decay curves of the prominent emitting states, $^3P_0$ and $^3P_1$ levels of Pr^{3+} and (d) partial energy level diagram of Pr^{3+} ions in YOF nanospheres, respectively.

a temperature adjustable stage of LINKAM instruments in the range of 90–580 K.

3. Results and discussion

Fig. 1 shows the structural and physical properties of YOF nanospheres prepared by sol-gel method. Fig. 1(a) represents the XRD pattern of the nanospheres in which all the patterns were identified to be in pure rhombohedral crystal system with the space group R-3 m and in concurrence with standard data (JCPDS card no. 04-011-8016). Raman scattering of the host YOF has been presented in Fig. 1(b) within the range 100–600 cm^{-1}. The Raman spectrum shows that the scattering of YOF includes bondages of Y-O and Y-F and the maximum phonon energy of the host YOF material is well below 500 cm^{-1} [5]. Fig. 1(c) gives the surface morphology of YOF nanospheres using SEM. It is found that all the particles are in spherical in shape, but agglomerated. Inset of Fig. 1(c) gives the particle size distribution using the SEM micrograph. The mean particle size from the size distribution curve is found to be ~44 nm. Fig. 1(d)–(g) present the EDS spectra of the YOF host and with the dopants too. The information in the EDS spectra were categorically presented in the insets of the figures. It has been observed that the composition and the concentration of the dopants were as per the expectations in the preparation of the samples.

Fig. 2 gives an overview of the emission characteristics of Pr^{3+} ion in YOF nanospheres. Fig. 2(a) represents the excitation spectrum of YOF:2%Pr where the emission being monitored at 657 nm ($^3P_0 \rightarrow {}^3F_2$). Excitation peaks arising from three transitions ($^3H_4 \rightarrow {}^3P_0$, $^3P_1$ and $^3P_2$) were observed in the region 430–510 nm. Among the three excitation transitions, $^3H_4 \rightarrow {}^3P_1$ is found to be the most intense. From the excitation spectrum, the energy difference between $^3H_4 \rightarrow {}^3P_0$ and $^3H_4 \rightarrow {}^3P_1$ was estimated by calculating the barycentres of the transitions and found to be 755.5 cm^{-1}. This value suggests that the two energy levels are thermally coupled and the emission transitions arising from these levels could be considered for further thermal sensing based on emission transitions [6,7].

Fig. 2(b) shows the concentration dependent emission spectra of Pr^{3+} in YOF when excited with 442 nm. Though there are several sharp peaks in the spectra, they can be classified into 9 different f-f transitions within Pr^{3+} ion. From higher to lower energy side in Fig. 2(b), the transitions appeared in the emission spectra were classified as $^3P_1 \rightarrow {}^3H_4$, $^3P_0 \rightarrow {}^3H_4$, $^3P_1 \rightarrow {}^3H_5$, $^3P_0 \rightarrow {}^3H_5$, $^3P_1 \rightarrow {}^3H_6$, $^3P_0 \rightarrow {}^3H_6$, $^3P_0 \rightarrow {}^3F_2$, $^3P_1 \rightarrow {}^3F_4$ and $^3P_0 \rightarrow {}^3F_4$ in the regions 469–472, 475–515, 515–550, 550–565, 600–620, 620–645, 650–665, 665–730 and 730–775 nm, respectively. In the Fig. 2(b) among emission spectra of three doping concentrations (1, 2 and 5 mol%) of Pr^{3+} in YOF, 2 mol% of Pr^{3+} showed the highest intensity. Concentration quenching has been observed after 2 mol% due to several cross-relaxation mechanisms [8] and hence YOF:2%

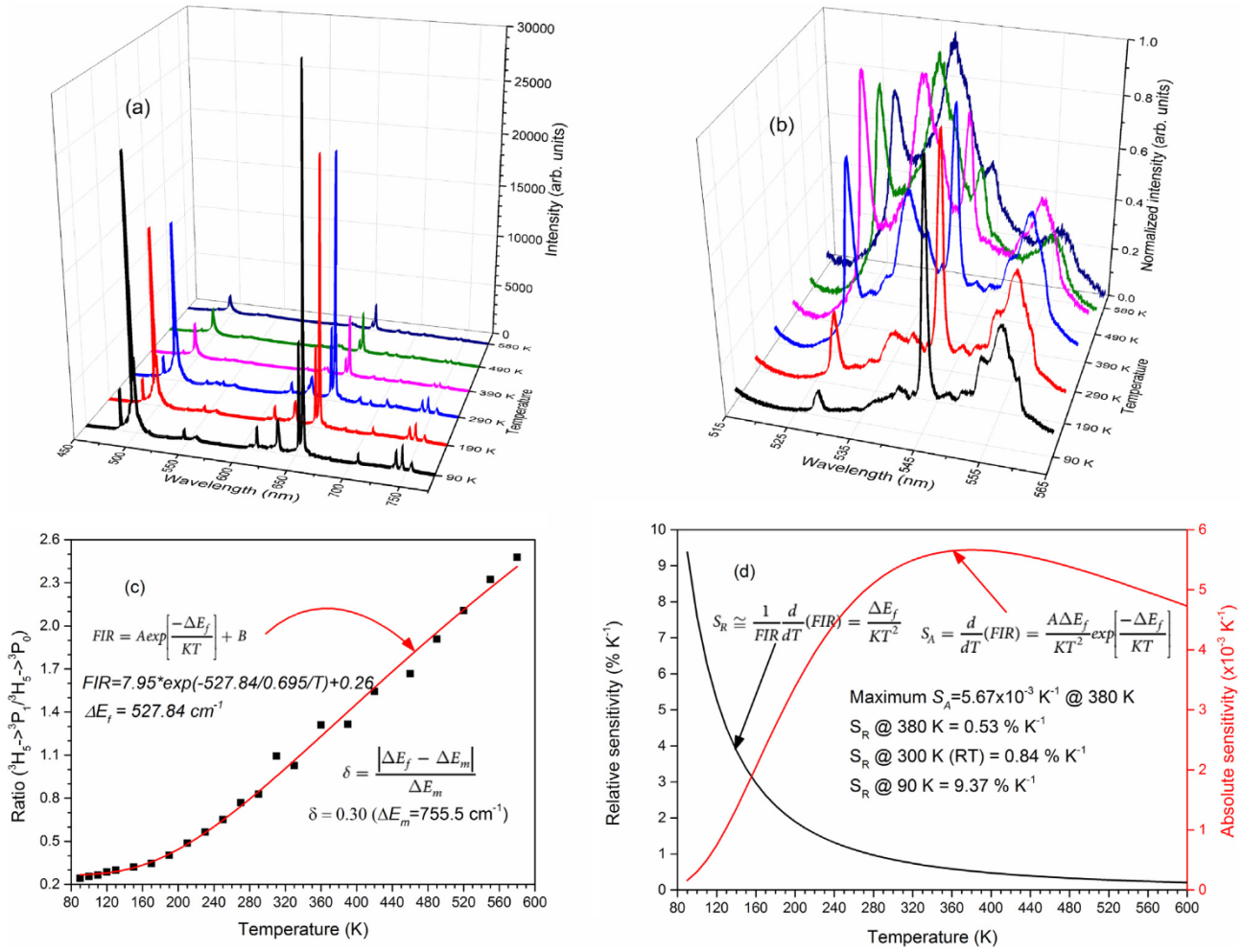

Fig. 3. Temperature-dependent (a) emission spectra in the region 450–775 nm, (b) normalized emission spectra in the region 515–565 nm, (c) FIR between $^3P_0 \rightarrow {}^3H_5$ and $^3P_1 \rightarrow {}^3H_5$ and (d) relative and absolute sensitivities in YOF:2%Pr, respectively.

Pr could be used for further temperature-dependent measurements. Of all the transitions, $^3P_0 \rightarrow {}^3H_4$ and $^3P_0 \rightarrow {}^3F_2$ is the most intense. As discussed earlier, a set of transitions arising from TCL to a similar terminating level could be used for temperature sensing. In this aspect, with the results available, four sets of transitions ($^3P_1$, $^3P_0 \rightarrow {}^3H_4$; $^3P_1$, $^3P_0 \rightarrow {}^3H_5$; $^3P_1$, $^3P_0 \rightarrow {}^3H_6$ and $^3P_1$, $^3P_0 \rightarrow {}^3F_4$) could be analysed. But of all the four sets, only one set ($^3P_1$, $^3P_0 \rightarrow {}^3H_5$) could be used for sensing analysis. There are several issues hindering the other sets from thermal sensing such as overlapping and ambiguity in assigning of transitions ($^3P_0 \rightarrow {}^3H_6$ and $^3P_1 \rightarrow {}^3F_2$), very low intensities at certain temperatures ($^3P_1 \rightarrow {}^3H_4$) and undistinguished transitions such as $^3P_1 \rightarrow {}^3F_4$ and $^3P_0 \rightarrow {}^3F_4$ and so on. Hence, only the intensities of the pair of transitions $^3P_1 \rightarrow {}^3H_5$ and $^3P_0 \rightarrow {}^3H_5$ between 515 and 550 and 550–565 nm, respectively could be used.

Decay lifetimes of the two luminescent levels $^3P_1$ and $^3P_0$ were found by measuring the decay curves by exciting at 470 nm and measuring the intensities of the transitions at 545 and 498 nm, respectively. They both are found to be double exponential due to influence of other transitions near to the monitoring wavelength that would not be so significant when considering emission intensities. The lifetimes for $^3P_1$ and $^3P_0$ energy levels were estimated to be 12.2 and 17.8 μs, respectively and are shown in Fig. 2(c) along with the double exponential fitting parameters.

Partial energy level diagram depicting excitation, emission channels in the YOF:Pr were shown in Fig. 2(d). It is interesting to note that a usual strong emission in Pr^{3+} ions in several other hosts at ~600 nm from $^1D_2$ energy level is absent in the present host. This may be due to the low phonon energy of the host material which hinders the process of de-excitation to $^1D_2$ from the higher energy levels [9]. A red arrow in Fig. 2(d), from $^3P_0$ to $^3P_1$ represents the thermal excitation of the $^3P_1$ level at higher temperatures according to Boltzmann's distribution law [7,10].

Fig. 3(a) represents the temperature-dependent emission spectra of YOF:2%Pr excited at 442 nm from 90 to 580 K in the entire emission region 450–775 nm. The spectra show that the overall intensities of all the emission peaks decreased with the increase in temperature. For clear perception, the spectra were presented for every 100 K though experimental data is after every 20/30 K.

Fig. 3(b) represents the normalized temperature-dependent emission spectra of YOF:2%Pr in the region 515–550 nm ($^3P_1 \rightarrow {}^3H_5$) and 550–565 nm ($^3P_0 \rightarrow {}^3H_5$). It is observed that the emission intensity of $^3P_1 \rightarrow {}^3H_5$ transition increases with the increase of temperature due to thermal excitation. Fig. 3(c) represents the ratio of intensities of the two transitions $^3P_1 \rightarrow {}^3H_5/{}^3P_0 \rightarrow {}^3H_5$ fitted according to the equation for FIR given elsewhere [3]. The absolute sensitivity of optical thermometry is the rate of change in the *FIR* in response to the temperature variation. Hence the absolute sensitivity (S_A) along with relative sensitivity (S_R) of the TCL were presented in Fig. 3(d) [3,11]. ΔE_f is the fitting energy difference between the TCL and the error with respect to experimental energy difference (ΔE_m) and this gives an in site of the agreement with the experimental values [3,7,12,13]. Fitting parameters and sensitivities are presented in the Fig. 3 and suggests that the material is having considerable S_R value for sensing of temperature. While the S_R value of YOF:Pr material is slightly less than that of their fluoride counterpart but it is very much comparable with the reported and hence could be a very interesting material for thermographic phosphor [4,14,15]. In this point of comparing different sensitivities, it could be analyzed from the FIR technique that due to the dependency of the relative sensitivity solely on the energy difference between the TCL, further improvement of sensitivities in the same host and dopant combinations could not be possible which tends to be the only limitation of the technique. However, search for various hosts with contrastive environments in which respective energy differences of TCL could lead to improved sensitivities.

4. Conclusions

Yttrium oxyfluoride (YOF) nanospheres with a mean diameter of ~44 nm were prepared by sol-gel method and the structure is revealed by XRD. Raman scattering reveals that the host matrix is having a very low phonon energy of ~480 cm^{-1}. SEM and EDS show the particle size distribution and composition, respectively. The fluorescence intensity of Pr^{3+} ions increases till 2% and then decreases due to concentration quenching mechanism. For 2 mol % of Pr^{3+} the FIR of the TCL $^3P_0$ and $^3P_1$ was determined with respect to temperature and found that the relative sensitivities of the material are 9.37 and 0.87% K^{-1} at 90 and 300 K, respectively and found to be comparable with the other reported host materials.

Declaration of Competing Interest

The authors declare that they have no known competing financial interests or personal relationships that could have appeared to influence the work reported in this paper.

Acknowledgements

This work is funded by national funds (OE), through FCT – Fundação para a Ciência e a Tecnologia, Portugal, I.P., in the scope of the framework contract foreseen in the numbers 4, 5 and 6 of the article 23, of the Decree-Law 57/2016, of August 29, changed by Law 57/2017, of July 19. This work was developed within the scope of the project i3N, UIDB/50025/2020 & UIDP/50025/2020, financed by national funds through the FCT/MEC.

References

[1] R. Tahara, T. Tsunoura, K. Yoshida, T. Yano, Y. Kishi, Jpn. J. Appl. Phys. 57 (2018) 6.
[2] T. Tsunoura, K. Yoshida, T. Yano, Y. Kishi, Jpn. J. Appl. Phys. 56 (2017) 6.
[3] S.A. Wade, S.F. Collins, G.W. Baxter, J. Appl. Phys. 94 (8) (2003) 4743–4756.
[4] M.S. Pudovkin, O.A. Morozov, V.V. Pavlov, S.L. Korableva, E.V. Lukinova, Y.N. Osin, V.G. Evtugyn, R.A. Safiullin, V.V. Semashko, J. Nanomater. 2017 (2017).
[5] J. Hölsä, B. Piriou, M. Räsänen, Spectrochim. Acta A 49 (4) (1993) 465–470.
[6] R. Kolesov, K. Xia, R. Reuter, R. Stöhr, A. Zappe, J. Meijer, P.R. Hemmer, J. Wrachtrup, Nat. Commun. 3 (2012) 1029.
[7] X. Wang, Q. Liu, Y. Bu, C.-S. Liu, T. Liu, X. Yan, RSC Adv. 5 (105) (2015) 86219–86236.
[8] J. Suresh Kumar, K. Pavani, T. Sasikala, B.C. Jamalaiah, M. Jayasimhadri, K.W. Jang, L. Rama Moorthy, Adv. Mater. Res. 123–125 (2010) 1235–1238.
[9] H. Chen, R. Lian, M. Yin, L. Lou, W. Zhang, S. Xia, J.-C. Krupa, J. Phys.: Condens. Matter 13 (5) (2001) 1151–1158.
[10] K. Pavani, J. Suresh Kumar, K. Srikanth, M.J. Soares, E. Pereira, A.J. Neves, M.P.F. Graça, Sci. Rep. 7 (1) (2017) 17646.
[11] S.F. León-Luis, U.R. Rodríguez-Mendoza, E. Lalla, V. Lavín, Sens. Actuat. B-Chem. 158 (1) (2011) 208–213.
[12] D. Jaque, F. Vetrone, Nanoscale 4 (15) (2012) 4301–4326.
[13] F. Wang, X. Liu, Chem. Soc. Rev. 38 (4) (2009) 976–989.
[14] M. Runowski, P. Woźny, I.R. Martín, V. Lavín, S. Lis, J. Lumin. 214 (2019).
[15] S. Zhou, G. Jiang, X. Wei, C. Duan, Y. Chen, M. Yin, J. Nanosci. Nanotechnol. 14 (5) (2014) 3739–3742.